Waveguide fabrication with integrated coupling optic

Thien Le Phu, David Le Coq, Pascal Masselin

Waveguide fabrication with integrated coupling optic

Thien Le Phu[a], David Le Coq[b], Pascal Masselin[a,*]

[a]*Laboratoire de Physico-Chimie de l'Atmosphère, Université du Littoral-Côte d'Opale, 189A avenue Maurice Schumann, Dunkerque, F-59140, , France*
[b]*Institut des Sciences Chimiques de Rennes, CNRS UMR 6226, Université de Rennes, , Rennes, F-35000, , France*

Abstract

We present the fabrication of a waveguide with integrated injection optics using a laser photoinscription technique in the bulk of a chalcogenide glass. The injection optic is a gradient index lens with a parabolic refractive index profile. Its focusing characteristics depend on the amplitude of the index gradient and the thickness of the lens. These two parameters can be used to optimize light injection when the lens is written in front of a waveguide. We show experimentally that the coupling efficiency can be superior to that obtained by conventional injection with an external lens. Numerical simulations show that this coupling efficiency can be as high as 85%. The simultaneous inscription of a waveguide and its injection lens result in a monolithic component that is compact, lightweight and insensitive to mechanical or thermal perturbations. Performance has been evaluated in the mid-infrared range, but these results can be extended to the visible.

1. Introduction

Lasers have become an important tool for materials processing in a wide variety of applications. In this context, spatial accuracy and resolution are greatly improved by the use of ultrashort-pulse lasers, as the nonlinear nature of the light-matter interaction in this case allows highly localized modification of the material. These properties are of great interest in particular for the development of micro-optics. In last decades, direct laser writing (DLW) has emerged as a powerful technique for additive manufacturing of three-dimensional (3D) miniaturized object via multiphoton polymerization in photoresist [1, 2]. The micro-component is built voxel by voxel that allows for precise control over the design even if the writing strategy should be adapted to minimize surface roughness.

Classical and Fresnel micro-lenses were first demonstrated in 2006 [3], followed by the realization of micro-lens array [4] and more complex micro-components, taking advantages of the versatility of the technique [5, 6, 7, 8]. Also one very interesting potential is the ability to assemble the micro-optical element directly on the tip of a fiber [9, 10, 11, 12] for collimation, intensity beam shaping as well as optical trapping.

Although the potential of DLW photopolymerization is significant, this technique suffers from absorption bands and of the dispersion of the material that degrade the performances of the optical micro-component. Similar approaches have also been used for additive manufacturing

*Corresponding author
Email address: pascal.masselin@univ-littoral.fr (Pascal Masselin)

of silica glass taking advantage of its optical quality while retaining the same capabilities in terms of precision and a spatial resolution reaching sub-micrometer scale [13, 14]. However, as with photopolymerization, the material undergoes shrinkage during post-processing, in this case annealing, that can be on the order of several percent. Therefore, this must be anticipated on a case by case basis when designing the component. Nevertheless, it could still result in some uncertainty about the final shape.

DLW can also be used as a subtractive manufacturing technique in hard materials. Here again, the inherent resolution of the method helps to produce very efficient micro-optics. However these results are obtained at the cost of complex experimental procedure, i.e. additional polishing [15], etching [16, 17] or cavitation for debris removal during the writing [18].

In addition to removing or adding matter, DLW can be used to locally modify the refractive index of bulk material [19], enabling the fabrication of a large number of functionalized photonic circuits in a wide variety of glass families [20]. As far as focusing micro-optical components are concerned, the literature describes mainly the realization of micro-lens with a first demonstration in 2002 of amplitude [21] and phase [22] Fresnel zone plate. The efficiency of diffraction has been increased to 57% at 632 nm by stacking layers of refractive index variation (Δn) to form multilevel diffractive lens [23]. A slightly higher diffraction efficiency reaching 60% at the same wavelength has been demonstrated with a more complex device consisting of two stacked multilevel lens with a separation between them but at the cost of rigorous design constraints [24].

The combination of the advantage of DLW in glass and the possibility to assemble micro-optics with guiding element as described previously for photopolymerisation could open up new possibilities for the realization of compact and robust photonic circuits. A first demonstration in this direction has been made in borosilicate glass [25]. In this article, the authors described the writing of a Fresnel zone plate placed in front of a waveguide and reported a coupling efficiency of 9%. They also shown the writing of three Fresnel zone plates slightly shifted transversaly. This results in three laterally shifted focal points and then the possibility to multiplex the beam into three different waveguides. However, the coupling efficiency obtained does not meet the requirements for practical applications.

Here, we propose an integrated structure that enables direct coupling of light into a waveguide, with measured efficiencies superior to conventional injection via an external lens, and numerically calculated values of the order of 85%. Moreover, because of the monolithic integration, the device is free of misalignment resulting from mechanical or thermal displacement.

The concept of the device is illustrated in figure 1. It consists of a gradient refractive index micro-lens (μGRIN) written in the bulk of glass and placed in front of a waveguide with uniform cross-section. In the next section we describe the concept of the μGRIN and how it was realized. A comprehensive evaluation of its focusing properties is also presented. The last section is devoted to the assembly of a μGRIN and a waveguide. We show that the coupling efficiency could be maximized by adjusting the μGRIN thickness and its refractive index profile.

2. Coupling optics

Basically the lens is made up of cylinders of refractive index variation Δn placed parallel to each other on a hexagonal mesh as shown on the left-hand part in figure 1, each cylinder having a different amplitude of Δn. These cylinders were realized as follows. At first, the sample is moved in order to place a Δn channel in front of the focal point of the laser. Then the sample is irradiated by a femtosecond pulse train during a time τ in a static position. The result is an increase of the

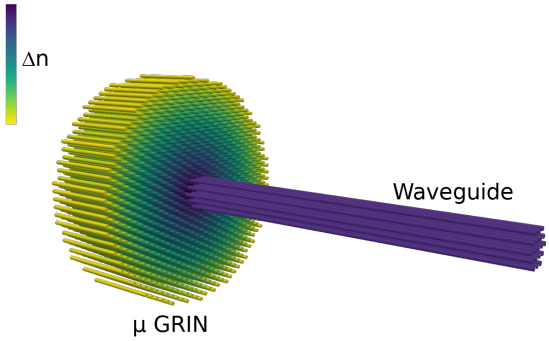

Figure 1: Illustration of the concept of our device. A graded-index lens, consisting of an alignment of rods, each with a different refractive index, is placed in front of a waveguide, itself made up of rods with the same index. The radial profile of the index distribution on the μGRIN rods is parabolic.

length of the channel. After that, the sample is moved perpendicularly to the writing beam so that the focal point is in front of the next channel. Then a new irradiation is performed and the operation is repeated for all the channels composing the cross section of the μGRIN. Next, the sample is then moved back parallel to the beam, and another slice is inscribed in the same way until the μGRIN reaches the desired thickness.

The most important parameter of the writing procedure is the duration of irradiation τ. We have shown in [26] with similar experimental conditions that the magnitude of Δn strongly depends on this simple experimental parameter as shown in figure 2. In this figure, Δn values measured by quantitative phase microscopy [27] are represented as a function of τ. Therefore one can see that the amplitude of Δn can easily be set individually for each channel by varying the value of τ. Here τ has been adjusted so that the overall refractive index profile of the entire structure is parabolic with the distance from the center.

In our experiments, lenses were produced according to this concept in a glass of composition $90\,[\,80\,GeS_2 - 20\,Ga_2S_3] - 10\,CsCl$. The glass has been synthesized by usual melt-quenching method [28]. High purity raw materials (Ga 7N, Ge and S 5N and CsCl 4N) were melted at 850°C under vacuum in a silica tube for several hours before being quenched in cold water. After synthesis, the glass is cut and polished to optical quality, using calcined aluminium oxide abrasive of size 3 and 0.03 μm. Its refractive index is equal to 2.030 [29] at a wavelength of 4.5 μm.

Irradiation was performed using a regenerative amplifier (Coherent RegA) as the source of 800 nm femtosecond pulses. The pulses have a duration of ~250 fs and are delivered at a repetition rate of 250 kHz. We used the external trigger function of the amplifier to control this repetition rate and also the irradiation time. The average power was set to 20 mW for all the channels since the magnitude of Δn is independent of this parameter [30]. The beam was focused inside the sample by use of a lens having a focal length of 50 mm.

The hexagonal mesh forming the μGRIN has a spacing between two channels of 2.3 μm to ensure that the inscription of a channel is not disturbed by the presence of other channels, thus assuring the homogeneity of the photo-inscription. The total diameter of the μGRIN is equal to 120 μm. The irradiation time τ was set at 100 ms at the center of the μGRIN and 10 ms for the channels placed at the edge.

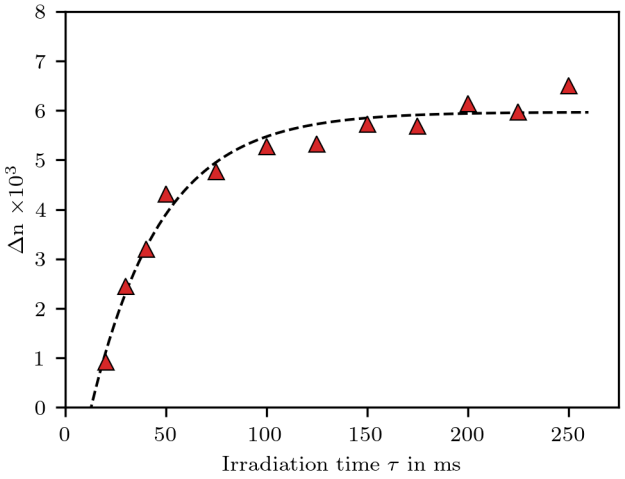

Figure 2: Dependence of the magnitude of the refractive index variation with the irradiation time τ. Measurements were taken in the visible range by a quantitative phase microscopie [27]. They represent the average value of Δn between 550 and 850 nm.

The light propagation through the μGRIN was also numerically simulated using the PyMeep python package implementing the finite-difference time-domain method (FDTD) for computational electromagnetic [31].

Focusing properties of the μGRIN are evaluated by measuring the beam profile after the μGRIN at different distances from it [32]. A quantum cascade laser at 4.5 μm is used as a source. Its beam first passes through a spatial filter and is then extended to a diameter of $\sim$1 cm, so that the wave in front of the sample can be considered a plane wave. The transmitted beam is imaged by a lens tube consisting of an aspherical lens (f = 6 mm) and an objective (f = 25 mm F2.5) onto the sensor of a FLIR A6750sc infrared camera. The spatial resolution of the system is evaluated at 0.8 μm/pixel. The camera is mounted on a translation stage with its axis of motion parallel to the beam. An image is recorded every 50 μm moving away from the sample. The images are then post-processed to reconstruct the beam.

A comparison between the measurement of light propagating through the μGRIN and its simulation is given in figure 3a and 3b, respectively. In both figures, the dashed line represents the sample surface. These figures are typical of the behavior observed for different μGRIN thicknesses. The focusing effect is clearly observed, with good agreement between measurements and numerical simulations. We characterized the focus by reporting the effective focal length (EFL) and the full width at half maximum (FWHM) of the beam at the focal point. The focal point is defined as the point of maximum intensity, and the EFL represents the distance between that point and the μGRIN surface. A typical beam profile at the focal point is shown in figure 4.

The EFL and the FWHM have been measured for different μGRIN thicknesses and their values are reported in the figures 5a and 5b, respectively, as well as the results of the simulations. It can be seen that as the thickness increases both the EFL and the FWHM decrease. It is worth to mention that for values of the thickness larger than those shown in the figure 5, the focusing occurs directly on the μGRIN surface, which may be interesting for applications other than those we are concerned with in this article. Focusing behavior with thickness is easily understood by considering that as the μGRIN becomes thicker, the phase difference accumulated between

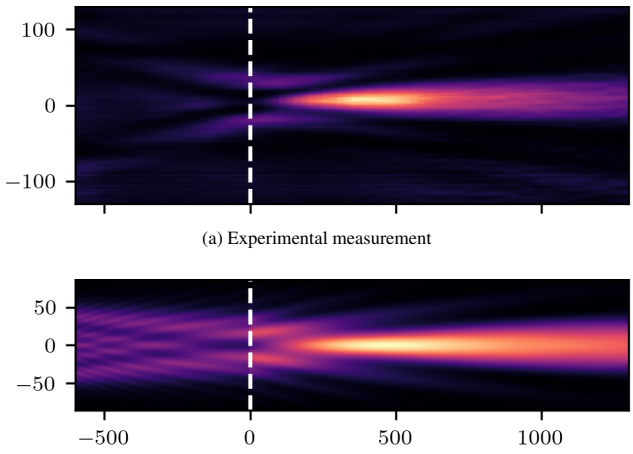

(a) Experimental measurement

(b) Numerical simulation

Figure 3: Comparison between experimental measurement of the light propagation and its numerical simulation for a μGRIN diameter of 120 μm and a thickness of 900 μm. The dashed lines represent the μGRIN surface. The μGRIN is located on the left of the line and the light propagates from left to right.

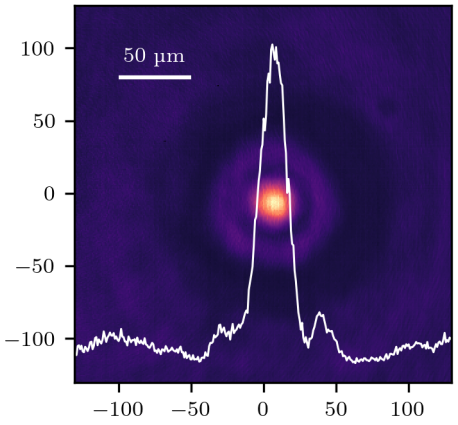

Figure 4: Image of the measured beam profile at the focal point. The distance are given in μm.

the center of the beam and its outer region is more important. As a result, the curvature of the wavefront is larger, leading to a shorter EFL and a tighter focusing.

One can observed on the figure 5a and 5b that the experimental measurements represented by the symbols are well described by the results of the simulation (plain lines) even if some discrepancy could be seen. This could be explained by several factors. First, the simulation were performed with a plane wave as input while some curvature of the wave front could remain even if the beam has been expanded. In addition, the actual magnitude of Δn in the mid-infrared region is not known. The values reported on the figure 2 have been measured in the visible. For the simulation in the mid-infrared, a better agreement between simulation and experimental data is obtained for Δn = 0.0015 which tends to indicate a decrease of Δn with the wavelength.

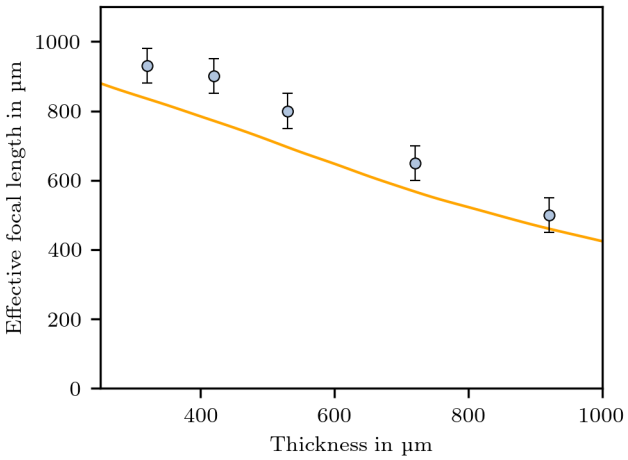

(a) Effective focal length

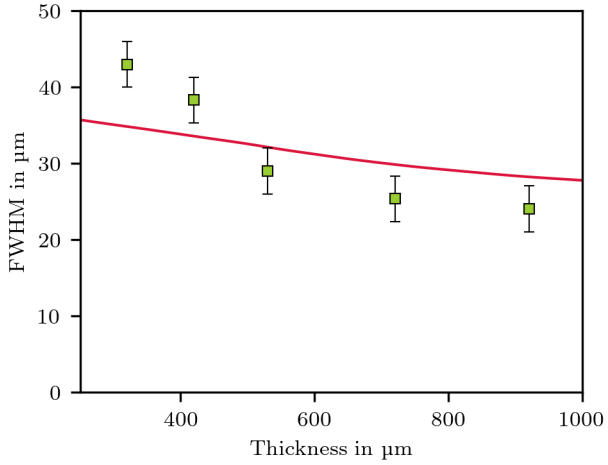

(b) Full width at half maximum of the beam waist

Figure 5: Dependence of the focus characteristics with the μGRIN thickness. Lines correspond to the simulated values and the symbols to the measured one.

3. μGRIN and waveguide assembly

In a second step, this μGRIN was inscribed on top of a waveguide and the coupling efficiency of light in the guide was studied. For this purpose, the same μGRIN as described above has been written simultaneously with a waveguide (with no spacing between them) that is also made up of Δn channels on the same hexagonal mesh, but with an identical irradiation time τ of 100 ms and then the same Δn for all channels. It has a diameter of 23 μm to minimize propagation losses [33] and a length of 15 mm. Another guide was also inscribed in the same glass substrate and with the same experimental parameters, but without the μGRIN. We use this guide as a reference to compare the power carried by our μGRIN and waveguide combination (G-WG) with conventional injection into an identical guide using an external lens. When testing the G-

WG device, the beam was also slightly focused for a better covering of the surface of the μGRIN in order to facilitate the measurements and to improve their accuracy. On the other hand the front face of the sample has been polished to form a slight 6° wedge to avoid retro-reflection of the beam towards the QCL laser. However, this leads to non-optimal injection conditions which implies that the coupling efficiency could reach a higher value than the one reported here.

After the waveguide, the beam is collimated using a ZnSe lens with a focal length of 12.7 mm. The coupling efficiency is evaluated by measuring the output power of the guide at a distance of approximately 1 m using a powermeter. The measured values were normalized to the power carried by the simple guide (without μGRIN). The results obtained for different μGRIN thickness values are represented by circles in Fig. 6. As evidenced in this figure, there is an optimum thickness value which leads to a coupling efficiency that is even higher than that obtained with conventional injection. The maximum absolute efficiency measured experimentally is 54%, corresponding to 70% after correction for reflection losses on the input and output faces.

This high value can be attributed to several factors. The first is the perfect lateral positioning of the lens in respect of the guide. Secondly, there is also a very good match between the dimensions of the focused beam and those of the guide. It should be noted that the diameter of the guide is suited to single-mode propagation with minimal propagation losses. Agreement with the dimensions of the focused beam is achieved by adapting the amplitude of the μGRIN's refractive index profile. The focal point is also optimally positioned with the guide entry, by adjusting the thickness of the μGRIN. Finally, the beam divergence after focusing is low, which facilitates injection.

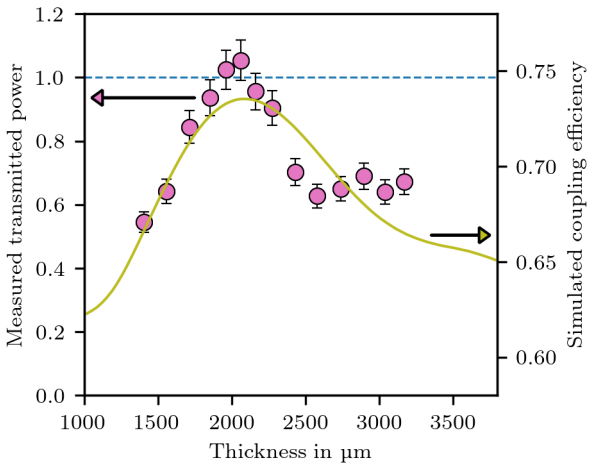

Figure 6: Measured transported power (circles) normalized to conventional injection with focusing optics positioned in front of the waveguide, and simulated coupling efficiency (solid line) for a µGRIN and waveguide assembly.

The evolution of the coupling efficiency with the thickness was also numerically simulated. The simulations were carried out under the same conditions as for the μGRIN alone, in particular assuming that the incident light is a plane wave. The calculated coupling efficiency is represented by the solid line in the figure 6. So the two vertical axes in this figure represent two slightly different things, but the superposition of the experimental values and the simulations clearly shows the concordance of the measured and simulated behaviors. As one might expect, the

results of these simulations show that the optimum thickness of the μGRIN corresponds to a focus at the entrance to the guide, as illustrated in figure 7. It can be seen in the figure 7a that when the thickness is too small, focusing takes place after the entry face of the guide, resulting in scattering at this point and therefore a reduction in the energy transported. On the other hand, when the thickness is too large (Fig.7c), the focal point is located in front of the guide entrance. The beam diverges before entering the guide, which also results in a reduction in transported power. The figure 7b represents the best situation, with focusing just at the entrance to the waveguide.

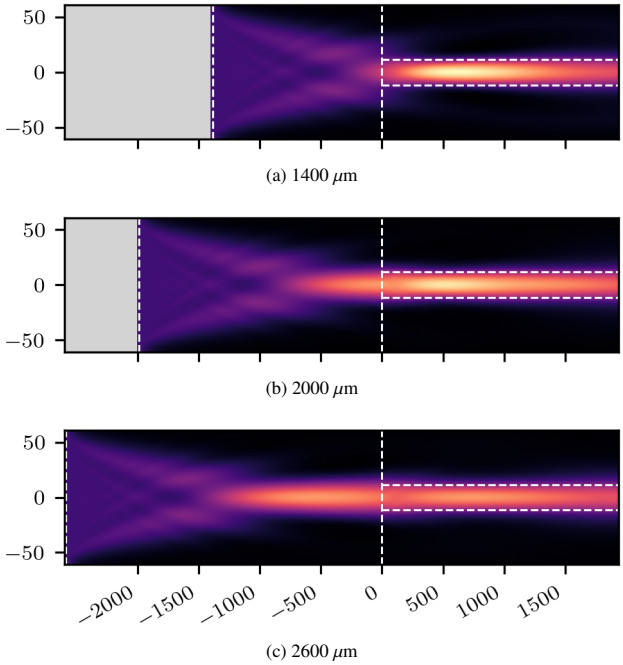

Figure 7: Numerical simulations of the coupling efficiency for different thicknesses. The vertical and horizontal dashed lines delimite the μGRIN and the waveguide, respectively. All the figures are horizontaly aligned on the input face of the waveguide.

On the other hand, the coupling efficiency depends also on the matching between the focusing conditions and the numerical aperture of the waveguide. To illustrate that point, we simulated the guided power for different values of the refractive index variation Δn. We use the same value of Δn for the waveguide and for the central value of Δn in the μGRIN. The results of these simulations are shown in figure 8. These values correspond to those obtained with the optimum thickness for each index contrast. The figure shows that the coupling efficiency can reach 85% for a structure with the characteristics used in our experiments. However, our experimental conditions do not allow us to obtain a value of Δn corresponding to the maximum coupling efficiency, but it should be emphasized that the values measured are already higher than those achieved by conventional injection. These results are therefore very encouraging for the experimental achievement of even higher coupling efficiencies.

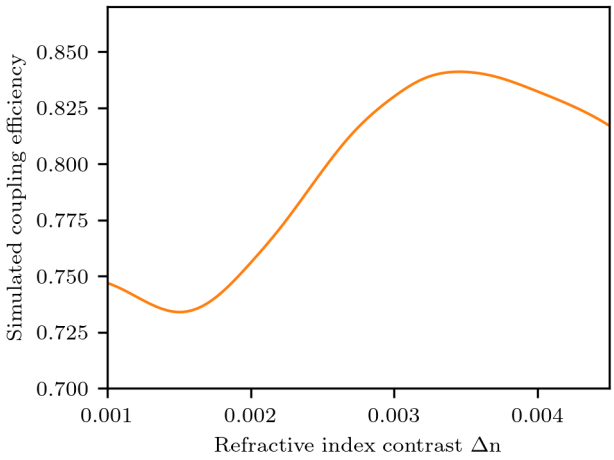

Figure 8: Simulation of coupling efficiency as a function of the refractive index variation amplitude Δn.

4. Conclusion

We have presented a new method for producing graded-index microlenses. The focusing properties of these micro-elements can be tailored simply by adjusting the thickness or amplitude of the refractive index contrast. When the μGRIN is placed on top of a waveguide, it forms a very compact and stable device that shows an improvement in the coupling efficiency compared to conventional injection with an external lens.

Numerical simulations show that this coupling efficiency can be as high as 85%. Moreover the design of the μGRIN that we used, is very simple but since it depends only on the irradiation duration τ, the refractive index profile of the coupling optic is not limited to parabolic. Therefore more complex profile like aspheric one or freeform lens, could be elaborated by use of inverse design technique [34] to further improve the coupling efficiency.

Finally we point out that we have chosen to highlight the behavior of our device in the mid-infrared spectral range in order to demonstrate the technique's potential for applications in this domain that would require efficient coupling of free-space light to a photonic circuit [35, 36, 37]. However, these results are not limited to this wavelength range, since the glass of the used composition is also transparent in the visible range, and photo-induced refractive index variation has also been demonstrated there. The concept of our device could therefore be extended to the near infrared and visible wavelengths.

Acknowledgments

The authors acknowledge the support of the French Research Agency (Agence Nationale de la Recherche, ANR) for its financial support of this work under the grant number ANR-22-CE08-0031. They also acknowledge the financial support of the French Ministry of Higher Education and Research and the Région Haut de France under the project CPER WaveTech. TLP acknowledge also the Université du Littoral-Côte d'Opale for the financial support of his work.

References

[1] M. Malinauskas, A. Žukauskas, S. Hasegawa, Y. Hayasaki, V. Mizeikis, R. Buividas, S. Juodkazis, Ultrafast laser processing of materials: from science to industry, Light: Science & Applications 5 (8) (2016) e16133.

[2] D. Gonzalez-Hernandez, B. Sanchez-Padilla, D. Gailevičius, S. C. Thodika, S. Juodkazis, E. Brasselet, M. Malinauskas, Single-step 3D printing of micro-optics with adjustable refractive index by ultrafast laser nanolithography, Advanced Optical Materials 11 (14) (2023) 2300258.

[3] R. Guo, S. Xiao, X. Zhai, J. Li, A. Xia, W. Huang, Micro lens fabrication by means of femtosecond two photon photopolymerization, Opt. Express 14 (2) (2006) 810–816.

[4] D. Wu, S.-Z. Wu, L.-G. Niu, Q.-D. Chen, R. Wang, J.-F. Song, H.-H. Fang, H.-B. Sun, High numerical aperture microlens arrays of close packing, Applied Physics Letters 97 (3) (2010) 031109.

[5] T. Gissibl, S. Thiele, A. Herkommer, H. Giessen, Two-photon direct laser writing of ultracompact multi-lens objectives, Nature Photonics 10 (8) (2016) 554–560.

[6] S. Thiele, K. Arzenbacher, T. Gissibl, H. Giessen, A. M. Herkommer, 3D-printed eagle eye: Compound microlens system for foveated imaging, Science Advances 3 (2) (2017) e1602655.

[7] C. R. Ocier, C. A. Richards, D. A. Bacon-Brown, Q. Ding, R. Kumar, T. J. Garcia, J. van de Groep, J.-H. Song, A. J. Cyphersmith, A. Rhode, A. N. Perry, A. J. Littlefield, J. Zhu, D. Xie, H. Gao, J. F. Messinger, M. L. Brongersma, K. C. Toussaint, L. L. Goddard, P. V. Braun, Direct laser writing of volumetric gradient index lenses and waveguides, Light: Science & Applications 9 (1) (2020) 196–.

[8] X. Porte, N. U. Dinc, J. Moughames, G. Panusa, C. Juliano, M. Kadic, C. Moser, D. Brunner, D. Psaltis, Direct (3+1)D laser writing of graded-index optical elements, Optica 8 (10) (2021) 1281–1287.

[9] T. Gissibl, S. Thiele, A. Herkommer, H. Giessen, Sub-micrometre accurate free-form optics by three-dimensional printing on single-mode fibres, Nature Communications 7 (1) (2016) 11763.

[10] J. Li, P. Fejes, D. Lorenser, B. C. Quirk, P. B. Noble, R. W. Kirk, A. Orth, F. M. Wood, B. C. Gibson, D. D. Sampson, R. A. McLaughlin, Two-photon polymerisation 3D printed freeform micro-optics for optical coherence tomography fibre probes, Scientific Reports 8 (1) (2018) 14789.

[11] A. Asadollahbaik, S. Thiele, K. Weber, A. Kumar, J. Drozella, F. Sterl, A. M. Herkommer, H. Giessen, J. Fick, Highly efficient dual-fiber optical trapping with 3D printed diffractive fresnel lenses, ACS Photonics (2019) 88 – 97.

[12] W. Hadibrata, H. Wei, S. Krishnaswamy, K. Aydin, Inverse design and 3D printing of a metalens on an optical fiber tip for direct laser lithography, Nano Letters 21 (6) (2021) 2422–2428, pMID: 33720738.

[13] X. Wen, B. Zhang, W. Wang, F. Ye, S. Yue, H. Guo, G. Gao, Y. Zhao, Q. Fang, C. Nguyen, X. Zhang, J. Bao, J. T. Robinson, P. M. Ajayan, J. Lou, 3D-printed silica with nanoscale resolution, Nature Materials 20 (11) (2021) 1506–1511.

[14] P.-H. Huang, M. Laakso, P. Edinger, O. Hartwig, G. S. Duesberg, L.-L. Lai, J. Mayer, J. Nyman, C. Errando-Herranz, G. Stemme, K. B. Gylfason, F. Niklaus, Three-dimensional printing of silica glass with sub-micrometer resolution, Nature Communications 14 (1) (2023) 3305.

[15] J. Dudutis, J. Pipiras, S. Schwarz, S. Rung, R. Hellmann, G. Račiukaitis, P. Gečys, Laser-fabricated axicons challenging the conventional optics in glass processing applications, Opt. Express 28 (4) (2020) 5715–5730.

[16] X.-Q. Liu, L. Yu, S.-N. Yang, Q.-D. Chen, L. Wang, S. Juodkazis, H.-B. Sun, Optical nanofabrication of concave microlens arrays, Laser & Photonics Reviews 13 (5) (2019) 1800272.

[17] J.-L. Skora, O. Gaiffe, S. Bargiel, J.-M. Cote, L. Tavernier, M. de Labachelerie, N. Passilly, High-fidelity glass micro-axicons fabricated by laser-assisted wet etching, Opt. Express 30 (3) (2022) 3749–3759.

[18] J.-G. Hua, H. Ren, J. Huang, M.-L. Luan, Q.-D. Chen, S. Juodkazis, H.-B. Sun, Laser-induced cavitation-assisted true 3D nano-sculpturing of hard materials, Small 19 (24) (2023) 2207968.

[19] R. Osellame, G. Cerullo, R. Ramponi, Femtosecond Laser Micromachining: Photonic and Microfluidic Devices in Transparent Materials, Topics in Applied Physics, Springer, 2012.

[20] D. Tan, Z. Wang, B. Xu, J. Qiu, Photonic circuits written by femtosecond laser in glass: improved fabrication and recent progress in photonic devices, Advanced Photonics 3 (2) (2021) 024002.

[21] W. Watanabe, D. Kuroda, K. Itoh, J. Nishii, Fabrication of Fresnel zone plate embedded in silica glass by femtosecond laser pulses, Opt. Express 10 (19) (2002) 978–983.

[22] E. Bricchi, J. D. Mills, P. G. Kazansky, B. G. Klappauf, J. J. Baumberg, Birefringent fresnel zone plates in silica fabricated by femtosecond laser machining, Opt. Lett. 27 (24) (2002) 2200–2202.

[23] K. Yamada, W. Watanabe, Y. Li, K. Itoh, J. Nishii, Multilevel phase-type diffractive lenses in silica glass induced by filamentationof femtosecond laser pulses, Opt. Lett. 29 (16) (2004) 1846–1848.

[24] P. Srisungsitthisunti, O. K. Ersoy, X. Xu, Volume Fresnel zone plates fabricated by femtosecond laser direct writing, Applied Physics Letters 90 (1) (2007) 011104.

[25] J. Choi, M. Ramme, M. Richardson, Directly laser-written integrated photonics devices including diffractive optical elements, Optics and Lasers in Engineering 83 (2016) 66–70.

[26] P. Masselin, E. Bychkov, D. Le Coq, Direct laser writing of a low-loss waveguide with independent control over the transverse dimension and the refractive index contrast between the core and the cladding, Opt. Lett. 41 (15) (2016) 3507–3510.
[27] E. Ampem-Lassen, S. T. Huntington, N. M. Dragomir, K. A. Nugent, A. Roberts, Refractive index profiling of axially symmetric optical fibers: a new technique, Opt. Express 13 (9) (2005) 3277–3282.
[28] J. Carcreff, P. Masselin, C. Boussard-Plédel, P. Kulinski, J. Troles, D. L. Coq, Step-index fibre from metal halide chalcogenide glasses, Opt. Mater. Express 10 (11) (2020) 2800–2812.
[29] A. Bréhault, Multispectral molded optics transparent in the visible and in thermal infrared, Ph.D. thesis, University of Rennes, France (2015).
[30] O. Caulier, D. Le Coq, L. Calvez, E. Bychkov, P. Masselin, Free carrier accumulation during direct laser writing in chalcogenide glass by light filamentation, Opt. Express 19 (21) (2011) 20088–20096.
[31] A. F. Oskooi, D. Roundy, M. Ibanescu, P. Bermel, J. Joannopoulos, S. G. Johnson, Meep: A flexible free-software package for electromagnetic simulations by the FDTD method, Computer Physics Communications 181 (3) (2010) 687–702.
[32] M. Baranski, S. Perrin, N. Passilly, L. Froehly, J. Albero, S. Bargiel, C. Gorecki, A simple method for quality evaluation of micro-optical components based on 3D IPSF measurement, Opt. Express 22 (11) (2014) 13202–13212.
[33] P. Masselin, E. Bychkov, D. Le Coq, Ultrafast laser inscription of high-performance mid-infrared waveguides in chalcogenide glass, IEEE Photonics Technology Letters 30 (24) (2018) 2123–2126.
[34] N. Barré, A. Jesacher, Inverse design of gradient-index volume multimode converters, Opt. Express 30 (7) (2022) 10573–10587.
[35] W. Chen, D. S. Venables, M. W. Sigrist, Advances in Spectroscopic Monitoring of the Atmosphere, 2021.
[36] K. Zou, K. Pang, H. Song, J. Fan, Z. Zhao, H. Song, R. Zhang, H. Zhou, A. Minoofar, C. Liu, X. Su, N. Hu, A. McClung, M. Torfeh, A. Arbabi, M. Tur, A. E. Willner, High-capacity free-space optical communications using wavelength- and mode-division-multiplexing in the mid-infrared region, Nature Communications 13 (1) (2022) 7662.
[37] L. Flannigan, L. Yoell, C.-Q. Xu, Mid-wave and long-wave infrared transmitters and detectors for optical satellite communications—a review, Journal of Optics 24 (4) (2022) 043002.